

Polarimetric variations of binary stars. II. Numerical simulations for circular and eccentric binaries in Mie scattering envelopes

N. Manset¹ and P. Bastien

Université de Montréal, Département de Physique, and Observatoire du Mont Mégantic, C.P. 6128, Succ. Centre-ville, Montréal, QC, H3C 3J7, Canada

manset@cfht.hawaii.edu, bastien@astro.umontreal.ca

ABSTRACT

Following a previous paper on Thomson scattering, we present numerical simulations of the periodic polarimetric variations produced by a binary star placed at the center of an empty spherical cavity inside a circumbinary ellipsoidal and optically thin envelope made of dust grains. Mie single-scattering (on spherical dust grains) is considered along with pre- and post-scattering extinction factors which produce a time-varying optical depth and affect the morphology of the periodic variations. The orbits are circular or eccentric. The mass ratio (and luminosity ratio) is equal to 1.0. We are interested in the effects that various parameters (grain characteristics, geometry of the envelope, orbital eccentricity, etc.) will have on the average polarization, the amplitude of the polarimetric variations, and the morphology of the variability.

We show that the absolute amplitudes of the variations are smaller for Mie scattering than for Thomson scattering, which makes harder the detection of polarimetric variations for binary stars surrounded by dust grains.

The average polarization produced depends on the grains' composition and size, and on the wavelength of observation. Among the four grain types that we have studied (astronomical silicates, graphite, amorphous carbon, and dirty ice), the highest polarizations are produced by grains with sizes in the range $a \sim 0.1 - 0.2 \mu\text{m}$ ($x = 2\pi a/\lambda \sim 1.0 - 2.0$ for $\lambda = 7000 \text{ \AA}$). Composition and size also determine if the polarization will be positive or negative.

In general, the variations are double-periodic (seen twice per orbit). In some cases, because spherical dust grains have an asymmetric scattering function, the polarimetric curves produced show single-periodic variations (seen once per orbit) in addition to the double-periodic ones. A mixture of grains of different sizes does not affect those conclusions.

Circumstellar disks produce polarimetric variations of greater amplitude (up to $\sim 0.3\%$ in our simulations) than circumbinary envelopes (usually $\lesssim 0.1\%$). Other geometries (circumbinary flared disks or prolate envelopes, and non-coplanar envelopes) do not present particularly interesting polarimetric characteristics.

¹Now at: Canada-France-Hawaii Telescope Corporation, P.O. Box 1597, Kamuela, HI 96743, USA

Another goal of these simulations is to see if the 1978 BME (Brown, McLean, & Emslie) formalism, which uses a Fourier analysis of the polarimetric variations to find the orbital inclination for Thomson-scattering envelopes, can still be used for Mie scattering. We find that this is the case, if the amplitude of the variations is sufficient and the true inclinations is $i_{\text{true}} \gtrsim 45^\circ$. For eccentric orbits, the first-order coefficients of the Fourier fit, instead of second-order ones, can be used to find almost all inclinations.

Subject headings: binaries: close — circumstellar matter — methods: numerical — techniques: polarimetric

1. Introduction

In the first paper (Manset & Bastien 2000, hereafter referred to as Paper I), we presented numerical simulations of the periodic polarimetric variations produced by a binary star surrounded by a circumbinary envelope composed of electrons. Thomson scattering was considered in an optically thin situation, along with pre- and post-scattering extinction factors which produce a time-varying (small) optical depth² and affect the morphology of the periodic variations by adding an additional harmonic to the variations. We studied the effects that orbital inclination, optical depth, geometry of the envelope and cavity, size and eccentricity of the orbits, and non-equal mass stars had on the average polarization level and the amplitude of the polarimetric variations.

We found that high polarization levels will result from a high inclination, a high optical depth, a flat envelope, or a big central cavity. Polarimetric variations are more apparent for a low inclination, a high optical depth, a flat envelope, a small cavity, or an orbit which brings the stars close to the inner edge of the cavity.

Using the formalism developed by Brown, McLean, & Emslie (1978, hereafter BME) the observations, or in this case the results of the numerical simulations, are fitted with a Fourier series with coefficients of orders zero, one, and two (see Equations 3 and 4 below). The first order coefficients from the fit (terms in 1λ) correspond to single-periodic variations (variations seen once per orbit), and those of second order (terms in 2λ) to double-periodic variations (seen twice per orbit). Those coefficients are used to find the orbital inclination (see Equations 5 and 6 below).

It was then shown that the BME formalism can be used to find the orbital inclination if it is $\gtrsim 45^\circ$, even though this formalism does not include variable absorption effects as in our simulations. The geometry (flatness of the envelope, size of the central cavity) and size of the orbit have no significant influence on the inclination found by the BME formalism.

An extension of the BME formalism for eccentric orbits has been performed by Brown, Aspin,

²Note: The optical depth has to be small to ensure that the assumption of single scattering in the envelope is not violated.

Simmons, & McLean (1982); however, their case considers a localized scattering region in eccentric orbit about a star, which is not a suitable geometry for the cases we want to study here. Therefore, we performed our own study of eccentric orbits.

For eccentric orbits, single-periodic variations appear for eccentricities as low as 0.10. As the eccentricity increases, these single-periodic variations dominate over the double-periodic ones. For low eccentricities, $e \lesssim 0.3$, the inclinations can be found with the first or second-order Fourier coefficients, if $i > 20^\circ$ and $i > 45^\circ$ respectively. For the high eccentricities, $0.3 < e < 0.6$, only the first-order coefficients should be used, if $i > 10^\circ$.

Orbital eccentricity is not the only factor that can introduce single-periodic variations: variable absorption effects, non equal mass stars, and asymmetric envelopes may also produce those.

In this second paper, we investigate the effects of scattering by spherical dust grains (Mie scattering). In addition to studying the influence of the optical depth and true orbital inclination already considered in Paper I, we also consider the effects of the composition and size of the dust grains on the level of polarization and the amplitude of the polarimetric variations. Our goal is to study the periodic polarimetric variations of binary young stars surrounded by envelopes in which dust grains are responsible for the scattering and polarization, and compare polarimetric observations with our numerical simulations.

As we have shown in Paper I that the BME formalism is still valid beyond its original limits (circular orbits, no extinction effects), now we also want to see if the BME formalism can be extended to the case of Mie scattering to find the orbital inclination, even though electrons and spherical dust grains have different scattering properties, and the BME formalism has been developed for Thomson scattering.

The simulations presented here are akin to the simulations where single-periodic polarimetric variations, usually double-peaked, are produced by a spotted star surrounded by a dusty circumstellar disk (see for e.g. Stassun & Wood 1999). Whereas in the latter case the polarimetric variations are produced by a pair of intrinsically polarized hot spots illuminating (and scattering off) the disk, here the variability is produced by the binarity of the source of light. The polarization produced by a single star surrounded by a circumstellar disk has been studied with Monte Carlo simulations, by, for e.g., Wood et al. (1996).

2. The scattering model

The scattering model used to compute the polarization and its position angle produced by two stars in orbit at the center of an ellipsoidal envelope was presented in Paper I. In addition to the parameters presented there (geometry of the envelope, orbit characteristics, optical depth, grid size), here we have to choose a grain composition (which will give a specific complex refractive index) and the size of the grains. Table 1 presents the characteristics of the grains studied in this

paper. A uniform size distribution was used for most of our simulations, but we also studied a distribution of grain sizes.

The calculations for Mie scattering use the following formulas:

$$Q = \frac{\tau_0 e^{\tau_0} \sum (\cos 2\beta)(i_2 - i_1) e^{-\tau_1 - \tau_2} dv/r^2 * iw}{\tau_0 e^{\tau_0} \sum (i_1 + i_2) e^{-\tau_1 - \tau_2} dv/r^2 + 2\pi \left(\frac{2\pi a}{\lambda}\right)^2 Q_{\text{ext}} \frac{x_{n0}}{n_{z\text{max}}}}, \quad (1)$$

$$U = \frac{\tau_0 e^{\tau_0} \sum (\sin 2\beta)(i_2 - i_1) e^{-\tau_1 - \tau_2} dv/r^2 * iw}{\tau_0 e^{\tau_0} \sum (i_1 + i_2) e^{-\tau_1 - \tau_2} dv/r^2 + 2\pi \left(\frac{2\pi a}{\lambda}\right)^2 Q_{\text{ext}} \frac{x_{n0}}{n_{z\text{max}}}}, \quad (2)$$

where:

τ_0 : optical depth in the equatorial plane of the envelope;

τ_1 : optical depth before scattering (between the light source and the scatterer);

τ_2 : optical depth after scattering (between the scatterer and the observer);

β : angle between the East–West direction and the scattering plane (which includes the light source, the scatterer and the observer);

ψ : scattering angle, between the light source, the scatterer and the observer;

r : distance between the light source and the scatterer;

dv : volume element (computed in relation to the grid size);

iw : weight which equals 1 if there is a scatterer, 0 otherwise;

$\frac{x_{n0}}{n_{z\text{max}}}$: optical depth per grid step;

a : radius of the spherical dust grain;

λ : wavelength of observation;

Q_{ext} : extinction cross section;

i_1 and i_2 : van de Hulst intensities.

Variable absorption effects are considered by using τ_1 and τ_2 . Depending on where the binary star is located inside the envelope, the optical depths between the source and the scatterer (τ_1), and between the scatterer and the observer (τ_2) will vary, and with them, the polarization. The van de Hulst intensities and Q_{ext} are calculated with the usual formulas that can be found in van de Hulst (1981, chap. 9) and make use of the complex refractive index of the grains.

The polarization P and its position angle θ are calculated from the Stokes parameters Q and U . When the polarization is produced by scattering, the sign used for P is related to its orientation with respect to the scattering plane (the plane containing the source of light, the scatterer, and the observer). A positive polarization is perpendicular to the scattering plane, whereas a negative one

is parallel to it. Thomson scattering always produces positive polarization, but both positive and negative polarization are produced by Mie scattering.

As in Paper I, a “canonical simulation” is a simulation which has the following parameters: an envelope with axis ratios 1.0, 1.0 and 0.25 (also referred to as a 25% flat envelope), a spherical cavity with radius 0.20 (also referred to as a 20% cavity), an optical depth of 0.1, and a grid size of 65. In addition, calculations are made for a wavelength of 7000 Å. Figure 1 presents a schematic view of this canonical geometry.

For further details on the calculations, see Paper I.

3. The BME formalism

The simulated polarimetric curves produced by the scattering model presented above are analyzed with the BME formalism, as in Paper I. For reference, we give the main formulas that are used. Observations are represented as first and second harmonics of $\lambda = 2\pi\phi$, where ϕ is the orbital phase ($0.0 < \phi < 1.0$):

$$Q = q_0 + q_1 \cos \lambda + q_2 \sin \lambda + q_3 \cos 2\lambda + q_4 \sin 2\lambda, \quad (3)$$

$$U = u_0 + u_1 \cos \lambda + u_2 \sin \lambda + u_3 \cos 2\lambda + u_4 \sin 2\lambda. \quad (4)$$

The inclination can be found with the first (Equation 5) or second (Equation 6) order Fourier coefficients, although it is expected for circular orbits that second order variations will dominate:

$$\left[\frac{1 - \cos i}{1 + \cos i} \right]^2 = \frac{(u_1 + q_2)^2 + (u_2 - q_1)^2}{(u_2 + q_1)^2 + (u_1 - q_2)^2}, \quad (5)$$

$$\left[\frac{1 - \cos i}{1 + \cos i} \right]^4 = \frac{(u_3 + q_4)^2 + (u_4 - q_3)^2}{(u_4 + q_3)^2 + (u_3 - q_4)^2}. \quad (6)$$

In an alternative representation, the eccentricity of the ellipse in the QU plane is related to the inclination. For the 2λ ellipse:

$$e = \frac{\sin^2 i}{2 - \sin^2 i}. \quad (7)$$

For the 1λ ellipse:

$$e = \sin i. \quad (8)$$

An important difference between this BME formalism and our numerical simulations is the inclusion of variable absorption effects in our work.

4. Mie Scattering, circular orbits: average polarization and amplitude of the polarimetric variations

4.1. Choice of grid size

As in Paper I, a preliminary step to the numerical calculations was to determine a suitable grid size, one with which the BME formalism would find an orbital inclination close enough to the real inclination (say, within $\approx 2^\circ$). Using astronomical silicates grains with radii of $0.1 \mu\text{m}$, we calculated models with grid sizes (radius) 25 to 95, by steps of 10. The results of the simulations, in which no noise was introduced, were used as input data for the BME equations. The orbital inclinations found in this manner are almost identical (within a few tenths of a degree) to those we found for Thomson scattering in Paper I. As in Paper I, we chose a grid size of 65, for which the inclination is within 1° of the true value, and the calculations can be performed in reasonable times.

4.2. Effects of the composition and size of the spherical dust grains

We made calculations for the canonical simulation (25% flat envelope, 20% central cavity, $\tau = 0.1$, grid radius=65), the four grain compositions listed in Table 1, and five grain radii (0.02, 0.05, 0.10, 0.2, and $0.50 \mu\text{m}$), at a wavelength of 7000 \AA . Since the polarization produced by Mie scattering depends on the size of the grain a and the wavelength of observation λ , it is common to introduce the parameter $x = 2\pi a/\lambda$; the values of x for the previously mentioned simulations are 0.18, 0.45, 0.90, 1.8, and 4.5. For each simulation, we used only one grain size and one grain composition.

If we compare the polarizing properties of dust grains and electrons, we note that dust grains (irrespective of composition and size) are less efficient polarizers than electrons. Grains also produce smaller absolute polarimetric variations per particle than electrons, although both electrons and grains produce about the same $\Delta P/P$ ratios; see Table 2. That important observation shows that for binary stars embedded in dust envelopes, periodic polarimetric variations should be harder to observe and detect.

For grain sizes of 0.02, 0.05 or $0.10 \mu\text{m}$ ($x = 0.18, 0.45, 0.90$), the highest polarization and polarimetric variations are found for astronomical silicates, followed by graphite and amorphous carbon, and finally dirty ice; grains made of dirty ice are 5–10 times less polarizing and produce variations about 5–10 times smaller than grains made of astronomical silicates. For grains with $a = 0.20 \mu\text{m}$ ($x = 1.8$), the dirty ice produces the highest polarization and variations. For $a = 0.5 \mu\text{m}$ ($x = 4.5$), astronomical silicates, graphite, and amorphous carbon have similar polarimetric properties, and dirty ices are less efficient polarizers. The highest polarizations are produced by grains with sizes in the range $\sim 0.1\text{--}0.2 \mu\text{m}$ ($x \sim 1.0\text{--}2.0$).

For astronomical silicates, we also did simulations for a wider range of grain sizes, going from

0.01 μm to 0.55 μm . The results are presented in Figure 2, where it is seen that the maximum polarization is reached for $x \approx 1.0$.

These results follow what is presented in Simmons (1982). See for example his figure 4 (polarization as a function of x for different grain compositions), where it can be seen that for silicate grains and ice, polarization depends on x with a very different behavior for these 2 grain compositions; a grain that is the most polarizing at one value of x will not necessarily be the most polarizing grain at other values of x .

Figure 6 in Simmons (1982) shows for silicate grains in particular how a different absorption coefficient changes the behavior of the polarization as a function of x . Finally, figure 5a shows that x_{max} , the value of x for which the polarization is maximum, depends on both the real and imaginary parts of the refractive index (and thus on the grain composition).

We also made some more calculations for astronomical silicates, adding grain sizes of 1.0 μm and 2.0 μm . Big grains ($a \geq 0.5\mu\text{m}$) are less efficient polarizers, as was already known (see for example Daniel 1978, Simmons 1983).

As shown by our simulations and by Simmons (1982), the average polarization produced by dust grains thus depends on the grain composition and size.

4.3. Polarization reversal

Polarization reversal (when the polarization goes from positive, or perpendicular to the scattering plane, to negative, or parallel to the scattering plane) seen in our simulations also occurs for the x values presented in Simmons (1982), figure 5b. For astronomical silicates, polarization reversal occurs at a value somewhere between $a = 0.19\mu\text{m}$ and $a = 0.25\mu\text{m}$, or $x \approx 1.8$ (see Figure 2), in agreement with figure 5b of Simmons (1982).

For dirty ice, we do not see any polarization reversal, which follows the figure 5b of Simmons (1982), except for our biggest grains ($a = 0.5\mu\text{m}$, $x \approx 4.5$) at low inclinations ($10^\circ \leq i \leq 30^\circ$). For the grains with large imaginary refractive index values (graphite and amorphous carbon), we see from table 1 of Daniels (1980) that polarization reversal is not expected at all, which is what is seen here, except in 2 cases for intermediate inclinations.

4.4. Distribution of grain sizes

We also studied a distribution of grain sizes, using the MRN size distribution $N(a) \sim a^{-3.5}$ (Mathis, Rumpel, & Nordsiek 1977) for astronomical silicates with sizes between 0.01 μm and 0.50 μm . The results are not very different from the case where only one grain size was considered. Since all polarimetric curves have the same morphology for a given set of parameters except grain

size, adding many of those curves only changes the polarization level, not the morphology.

4.5. Effect of true orbital inclination

As the inclination decreases from 90° (edge-on) to 0° (pole-on), the polarization decreases, in general following a theoretical law (developed for a single star at the center of an axisymmetric envelope but nonetheless interesting for our case) that can be found for example in Brown & McLean (1977): the residual polarization (sum of polarization of the scattered light and the unpolarized light from the star) scales as $\sin^2(i)$. Deviations from this theoretical law are found when the optical depth is high ($\tau = 0.5$, too high to consider single scattering only) or the grains are big ($a \geq 0.2 \mu\text{m}$, which probably introduces higher frequency variations in the polarization as a function of the scattering angle). With a 90° inclination, the U parameter is null, and only the Q parameter varies. As the inclination decreases, both the Q and U parameters vary, and more so as the inclination decreases. In general, the behavior is the same as for Thomson scattering.

4.6. Periodic polarimetric variations

The simulations for a binary star in a circumbinary envelope give polarimetric variations that are double sine waves (see Figure 3), which translate to an ellipse that is traced out twice per orbit in the QU plane. The average Stokes parameter U is zero, as is expected from a geometry oriented in the plane of the sky in a East–West direction, and the position angle is usually $\approx 0^\circ$, perpendicular to the projection of the envelope’s main axis and scattering angle.

In order to decrease the number of parameters influencing the polarization and isolate causes and their effects, we can take a look at the contribution of only one star instead of considering the combined effects of the 2 stars. In Figure 4 we show the polarimetric variations for the primary only, as if it were in orbit around an “invisible”, or much fainter, secondary star, both stars being in orbit at the center of the same circumbinary shell. Even though the orbit is circular, single-periodic variations are seen in addition to the usual double-periodic ones. We have shown in Paper I that variable absorption effects introduce such single-periodic variations; but if we neglect those variable absorption effects and impose a constant optical depth in our Mie simulations, those single-periodic variations persist. This is due to the asymmetric phase function of dust grains. It is also seen that the peaks of polarization are not located exactly at phases 0.25 and 0.75, as expected for an asymmetric phase function.

Therefore, in addition to variable absorption effects, non equal mass stars, orbital eccentricity, and asymmetric envelopes, Mie scattering can also cause single-periodic variations.

4.7. Effect of orbits and various geometries

Like the Thomson scattering results presented in Paper I, the amplitude of the variations increases significantly for larger size orbits. For an orbit that comes close to the inner edge of the circumbinary disk, the polarimetric variations are more apparent.

In order to see the effects of geometries different than a circumbinary ellipsoidal envelope, we made simulations for flared circumbinary disks, prolate circumbinary envelopes, and circumstellar disks. We also investigated the effects of a non-coplanar geometry where the plane of symmetry of the envelope and the orbital plane differ from one another.

First, we tried a geometry similar to a flared disk, with a conic opening (with half-angle between 10 and 80°) in an ellipsoidal envelope. As the angle of the cone increases, so does the polarization and amplitude of the variations. We also studied prolate geometries instead of oblate ones, orienting the long axis of the envelope along 3 axes (toward the observer, in a N–S and E–W orientation in the plane of the sky). Finally, we inclined the envelope by $\pm 30^\circ$ with respect to the orbital plane. For all those cases, polarization and amplitude of variations are affected to various degrees, but the polarimetric variations have the same morphology.

For circumbinary envelopes, the polarimetric curves we have produced so far seldom have an amplitude greater than 0.10%, whereas Simmons (1983) could produce amplitude of many tenths of a percent, or even of a few percents, with a geometry more favorable for high amplitude polarimetric variations: a single circumstellar envelope externally illuminated by only one star.

Indeed, the most interesting simulations were done with a circumstellar disk around the primary, a “naked” secondary which does not have any circumstellar material in its environment, and no circumbinary disk. See Figure 5 for an example of such a geometry. As expected from this more asymmetric geometry, the polarimetric variations produced have a greater amplitude, ranging from 0.1 to 0.3%. The primary star that sits in the middle of its circumstellar disk does not produce any variation, as expected, but numerical noise is present at a level of $\lesssim 0.01\%$ in polarization. Variations for the secondary star, which revolves around the primary and its disk, are a sum of double- and single-periodic variations.

5. Mie Scattering, circular orbits: finding the orbital inclination

Average polarization, amplitude of the polarimetric variations, and morphology of the variability are all interesting, but periodic polarimetric observations can potentially give an additional and very interesting parameter for a binary star: its orbital inclination, which is found by using the formalism developed by BME (Equations 5 and 6). We now investigate if their formalism, which was developed for Thomson scattering, circular orbits, and constant optical depth, can be extended successfully to our simulations to find the orbital inclination.

5.1. Effects of true orbital inclination, composition and size of the spherical dust grains on the orbital inclination found by the BME formalism

For an optical depth of 0.1, we have found that the BME formalism will work (i.e., true inclinations can be found from the BME analysis of the polarimetric variations if $i_{\text{true}} \gtrsim 45^\circ$) as long as there are polarimetric variations of sufficient amplitudes for the mathematical analysis (by sufficient, we mean for example, 0.002% for simulations without stochastic noise). The composition or the size of the grains is not important as long as some variations are introduced. Big grains ($a \gtrsim 0.5 \mu\text{m}$) do not produce enough variations for the BME analysis to work properly.

In general, the uncertainty on the inclination found by the BME formalism (calculated with the method of propagation of errors) is higher for dust grains than for electrons. This is understandable since, as stated before, grains produce smaller amplitude polarization variations, which will increase the uncertainty on the inclination found.

5.2. Optical depth effects

The effects of optical depths were studied for some combinations of grain composition and size, with optical depths of 0.02, 0.05, 0.2, and 0.5. As expected, the polarization increases with the optical depth, as does the amplitude of the polarimetric variations. All the simulations studied here produced polarimetric variations with sufficiently large amplitudes, so again, the BME formalism works for $i_{\text{true}} \gtrsim 45^\circ$.

Berger & Ménard (1997) have studied multiple Mie scattering in circumbinary shells with optical depths up to $\tau = 3.0$, and have found that even with such a high optical depth, the estimation of inclination from the BME formalism is still very good.

5.3. Effect of orbits and various geometries

Although the inclination found by the BME equations is not significantly affected by the geometry in the case of the flared disk geometry, it is more seriously affected for prolate geometries and non-coplanar orbital and geometric planes. For the prolate envelope inclined at 60° , the two cases where the long axis of the prolate envelope is in the plane of the sky give inclinations close to 60° , but for the long axis coming toward the observer, the inclination found is 10° too low. For the same inclination, the envelope inclined by $\pm 30^\circ$ with respect to the orbital plane gives orbital inclinations of 54° or 43° , significantly different than the 59° found for the coplanar case.

For the circumstellar disks, BME can find the inclination if it is $\geq 30^\circ$. The lower threshold, compared to the circumbinary case, might be due to the amplitude of the variations, which are greater for the circumstellar envelope geometry than for the circumbinary envelope geometry.

6. Mie scattering, eccentric orbits

To investigate the possible effects of non-circular orbits on polarimetric observations, canonical simulations were performed with orbital eccentricities of 0.1, 0.3, and 0.5. It should be noted that in these simulations, the orbital semi-major axes have been adjusted according to the eccentricity (i.e., decreased with increasing e) so the stars came at about the same distance from the inner edge of the envelope, irrespective of the eccentricity of their orbit (the maximum distance between the center of the envelope and any of the two stars was always ≈ 0.15). This was done so we could study the influence of the eccentricity without having to deal with the influence of how close the stars come to the inner edge of the circumbinary envelope. The results found for Mie scattering are identical to those we have found for Thomson scattering (see Paper I).

The eccentricity has no significant influence on the average level of polarization, but does change the amplitudes of the polarimetric variations: the amplitudes decrease as the eccentricity increases. As the eccentricity increases, the 2λ variations that are dominant for low eccentricities give way to 1λ variations. Moreover, higher harmonics appear; a fit with 1λ and 2λ is not sufficient to reproduce the polarimetric curves, so 3λ and 4λ harmonics are needed.

When looking at the inclinations found by the BME formalism with the second-order coefficients of the fit, we find that the true inclinations are found for the lower eccentricities ($0.1 < e < 0.3$) and the highest inclinations ($i_{\text{true}} \gtrsim 45^\circ$). For the highest eccentricity studied here, $e = 0.5$, the second-order coefficients can not be used to find the orbital inclination, as the BME formalism is unable to find the true inclination.

For all eccentricities, even the highest one studied here $e = 0.5$, the first-order coefficients can be used to find almost all inclinations. There is a numerical problem with the true inclination of 80° , for which the BME formalism can not assign the right inclination. The lowest inclinations ($i_{\text{true}} < 20^\circ$) are harder to find.

When the periastron is changed to values other than 0° , the results of the BME analysis are slightly modified. With an eccentricity of 0.5, the second-order and first-order coefficients now both give reasonable results for $i_{\text{true}} \gtrsim 45^\circ$.

7. Comparison between the numerical simulations and polarimetric observations of binary young stars

In future papers, we will present polarimetric observations of binary young stars, which are objects surrounded by circumstellar material (dust grains). The binaries we have selected have short periods, so we believe the geometry adopted here (circumbinary ellipsoidal envelope with a central cavity) is suitable for these kinds of objects.

Some of the observed pre-main sequence binaries show periodic polarimetric variations, al-

though they are in general of lower amplitude and less clear than those of binary hot stars (surrounded by electrons), such as Wolf–Rayet stars (see, for example, St-Louis et al. 1988; Drissen et al. 1989b; Robert et al. 1990). This is in agreement with our previous comparison of the polarimetric properties of electrons and dust grains.

Non-periodic polarimetric variations that are known to exist even for single young stars (Bastien 1982; Drissen, Bastien, & St-Louis 1989a; Ménard & Bastien 1992) produce stochastic noise in the polarimetric curves of binary young stars, sometimes hiding the low amplitude periodic variations.

The small amplitude variations ($\lesssim 0.10\%$) often seen in binned data can be caused by non favorable inclinations or geometry, or not enough scatterers, but we believe it is in general agreement with one of our conclusions, that dust grains produce smaller amplitude variations than electrons.

Some stars do have high amplitude polarimetric variations of up to 0.7%. Such large amplitudes were not quite produced by our simulations, although circumstellar disks, a more favorable geometry than circumbinary disks, do produce more substantial variations, up to $\sim 0.3\%$. For the observed high amplitude polarimetric variations, a circumbinary envelope might thus not be an adequate geometry and circumstellar envelope(s)/disk(s) could be present.

8. Discussion

We have presented numerical simulations of the periodic polarimetric variations produced by a binary star placed at the center of an empty cavity in a circumbinary ellipsoidal and optically thin envelope. Mie single-scattering in envelopes made of single-size and single-composition grains was considered. The orbits were circular or eccentric. The mass ratio (and luminosity ratio) was equal to 1.0. These parameters are to represent short-period spectroscopic binary young stars that are embedded in a circumbinary envelope and have evacuated the central regions of this envelope due to gravitational or radiative interactions.

We have shown that the absolute amplitude of the variations is smaller for Mie scattering than for Thomson scattering, which will render more difficult the detection of polarimetric variations in binary stars surrounded by dust grains. In fact, polarimetric observations of binary young stars that will be presented in future papers show periodic variations that are sometimes much less obvious than for hot stars, for example. This may be due in part to the scattering properties of dust grains, although other factors, such as orbital inclination or scattering geometry, can also decrease (or increase) the amplitude of the polarimetric variations.

The average polarization produced depends on the grains' composition (through the real and imaginary parts of the refractive index) and size, and on the wavelength of observation; a highly polarizing grain at a given grain size will not necessarily polarize as efficiently if it is smaller or bigger. For the four grain compositions that we have studied (astronomical silicates, graphite,

amorphous carbon, and dirty ice), the highest polarizations are produced by grains with sizes in the range $\sim 0.1\text{--}0.2\ \mu\text{m}$ ($x \sim 1.0\text{--}2.0$ for $\lambda = 7000\ \text{\AA}$).

Polarization reversal was seen for astronomical silicates (at $a \approx 0.2\ \mu\text{m}$, or $x \approx 1.8$), but not for dirty ices, graphite, and amorphous carbon grains, which is in agreement with previous works (Simmons 1982; Daniels 1980).

The periodic variations produced are in general double-periodic (seen twice per orbit), although we have shown that variable absorption effects (pre- and post-scattering factors), non equal mass stars, orbital eccentricity, asymmetric envelopes, and Mie scattering (on spherical dust grains, which have an asymmetric scattering function) introduce single-periodic variations (seen once per orbit).

We have also studied a mixture of grains whose sizes followed a MRN distribution; this did not affect the morphology of the polarimetric variations.

Circumstellar disks are more interesting than circumbinary disks, in the sense that they produce polarimetric variations that are more readily detectable ($\sim 0.3\%$ versus $\lesssim 0.1\%$). Other geometries (flared disks, prolate envelopes, non-coplanar disks) did not produce any difference in the morphology or amplitude of the variations.

We have shown that the BME formalism is still valid beyond its original limits (circular orbits, no extinction effects, Thomson scattering), under certain circumstances. In general, the BME formalism will be able to find the orbital inclination if this inclination is $\gtrsim 45^\circ$ and if the amplitude of the polarimetric variations is sufficient. The composition or the size of the grains is not important as long as some variations are introduced, but the inclinations found by the BME formalism seem to be affected by prolate and non-coplanar geometries.

The second-order Fourier coefficients of the fit can be used for the lower orbital eccentricities ($0.1 < e < 0.3$) and the highest inclinations ($i_{\text{true}} \gtrsim 45^\circ$). For all eccentricities, even the highest one studied here $e = 0.5$, the first-order coefficients can be used to find almost all inclinations.

Comparisons between polarimetric observations of binary stars and these simulations will help understand these systems (presence of circumbinary and/or circumstellar disks, geometry of the envelope, orbital eccentricity, etc.) although the interpretations might not be unique, as many parameters can have similar effects on the polarimetric variations (mainly the amplitude and the presence of single-periodic variations). In that case, other types of observations (imaging and spectroscopy) would nicely complement polarimetric ones.

If the observations are of high enough quality and show variations of sufficient amplitude, the BME formalism can be used to determine the orbital inclination, a fundamental parameter for these stars.

N. M. would like to thank the Conseil de Recherche en Sciences Naturelles et Génie of Canada, the Fonds pour la Formation de Chercheurs et l’Aide à la Recherche of the province of Québec,

the Faculté des Etudes Supérieures and the Département de physique of Université de Montréal for scholarships, and P. B. for financial support. N. M. would also like to thank F. Ménard for numerous discussions. We would like to thank the Conseil de Recherche en Sciences Naturelles et Génie of Canada for supporting this research.

REFERENCES

- Bastien, P. 1982, *A&AS*, 48, 153
- Berger, J.-P., & Ménard, F. 1997, in *IAU Symposium 182, Low Mass Star Formation – from Infall to Outflow*, ed. F. Malbet & A. Castets, 201
- Brown, J. C., & Mclean, I. S. 1977, *A&A*, 57, 141
- Brown, J. C., McLean, I. S., & Emslie, A. G. 1978, *A&A*, 68, 415
- Brown, J. C., Aspin, C., Simmons, J. F. L., & McLean, I. S. 1982, *MNRAS*, 198, 787
- Daniel, J.-Y. 1978, *A&A*, 67, 345
- Daniel, J.-Y. 1980, *A&A*, 87, 204
- Drissen, L., Bastien, P., & St-Louis, N. 1989a, *AJ*, 97, 814
- Drissen, L., Robert, C., Lamontagne, R., Moffat, A. F. J., St-Louis, N., van Weeren, N., & van Genderen, A. M. 1989b, *ApJ*, 343, 426
- Draine, B. T. 1985, *ApJS*, 57, 587
- Greenberg, J. M. 1968, in *Nebulae and Interstellar Matter*, ed. B. M. Middlehurst & L. H. Aller (Chicago: University of Chicago Press), 221
- Manset, N., & Bastien, P. 2000, *AJ*, 120, 413 (Paper I)
- Mathis, J. S., Rumpl, W., & Nordsieck, K. H. 1977, *ApJ*, 217, 425
- Ménard, F., & Bastien, P. 1992, *AJ*, 103, 564
- Robert, C., Moffat, A. F. J., Bastien, P., St-Louis, N., & Drissen, L. 1990, *ApJ*, 359, 211
- Rouleau, F., & Martin, P. G. 1991, *ApJ*, 377, 526
- Simmons, J. F. L. 1982, *MNRAS*, 200, 91
- Simmons, J. F. L. 1983, *MNRAS*, 205, 153
- Stassun, K., & Wood, K. 1999, *ApJ*, 510, 892
- St-Louis, N., Moffat, A. F. J., Drissen, L., Bastien, P., & Robert, C. 1988, *ApJ*, 330, 286
- van de Hulst, H. C. 1981, *Light Scattering by Small Particles* (New York: Dover Publications, Inc.)
- Wickramasinghe, N. C. 1967, *Interstellar Grains*, (London: Chapman and Hall Ltd.)
- Wickramasinghe, N. C., & Guillaume, C. 1965, *Nature*, 207, 366

Wood, K., Bjorkman, J. E., Whitney, B. A., & Code, A. D. 1996, *ApJ*, 461, 828

This preprint was prepared with the AAS L^AT_EX macros v5.0.

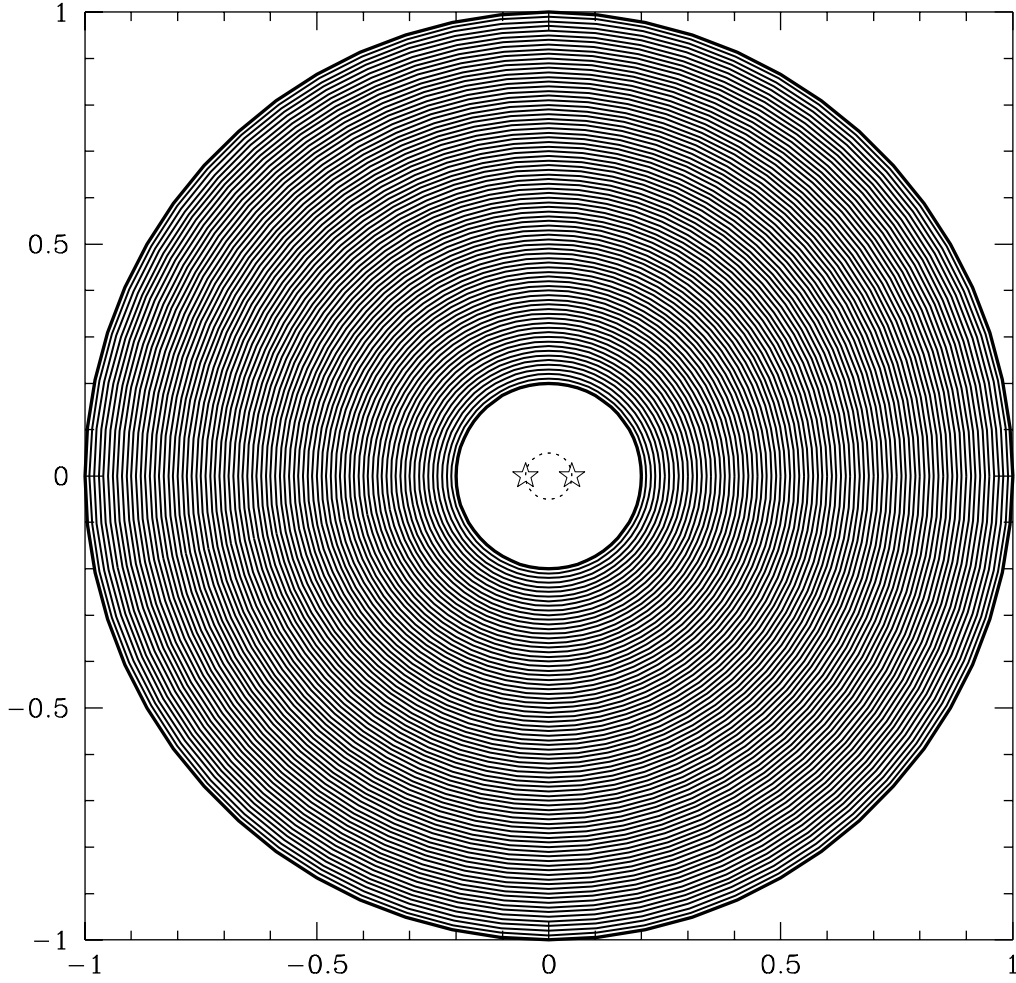


Fig. 1.— Pole-on view of a circumbinary envelope with a cavity size 20% of the envelope size. An equal-mass binary with an orbital radius 5% of the envelope size is placed at the center of the cavity.

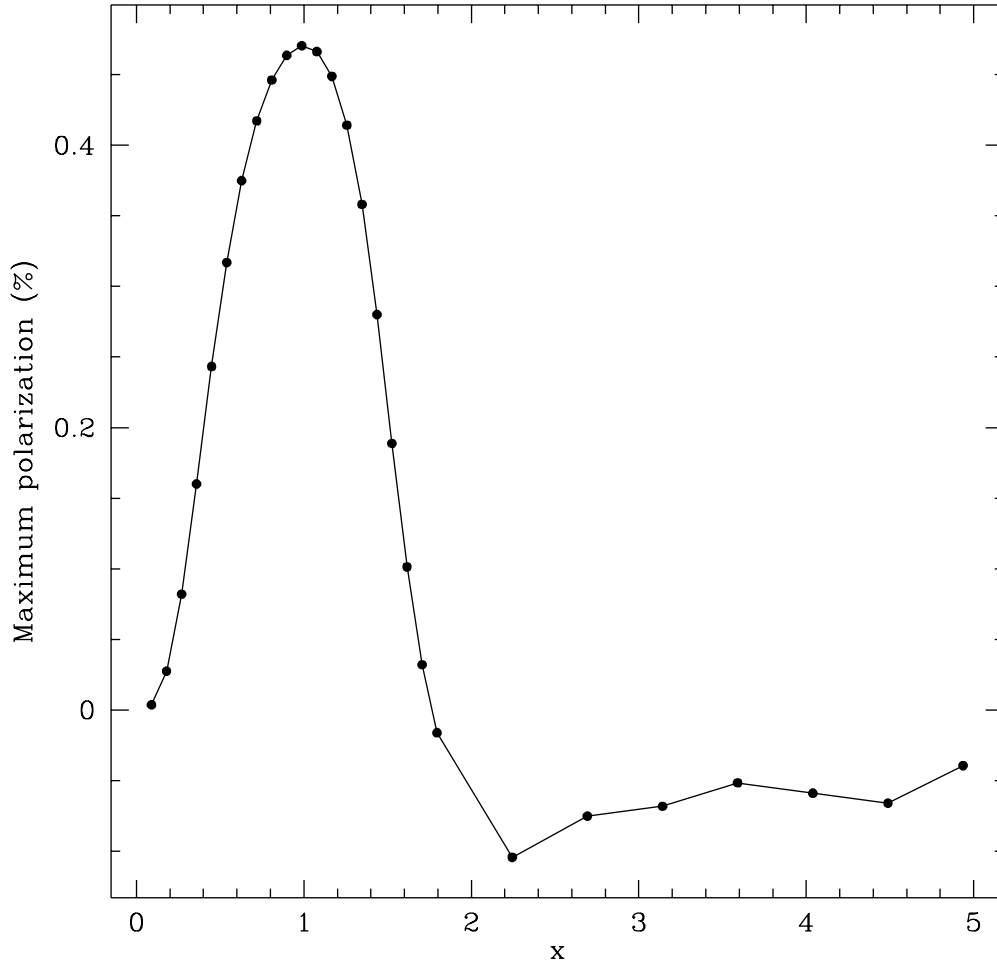


Fig. 2.— For astronomical silicate grains, polarization as a function of $x = 2\pi a/\lambda$. The highest polarization occurs for $x \approx 1.0$. Polarization reversal occurs at a value somewhere between $a = 0.19 \mu\text{m}$ and $a = 0.25 \mu\text{m}$, or $x \approx 1.8$.

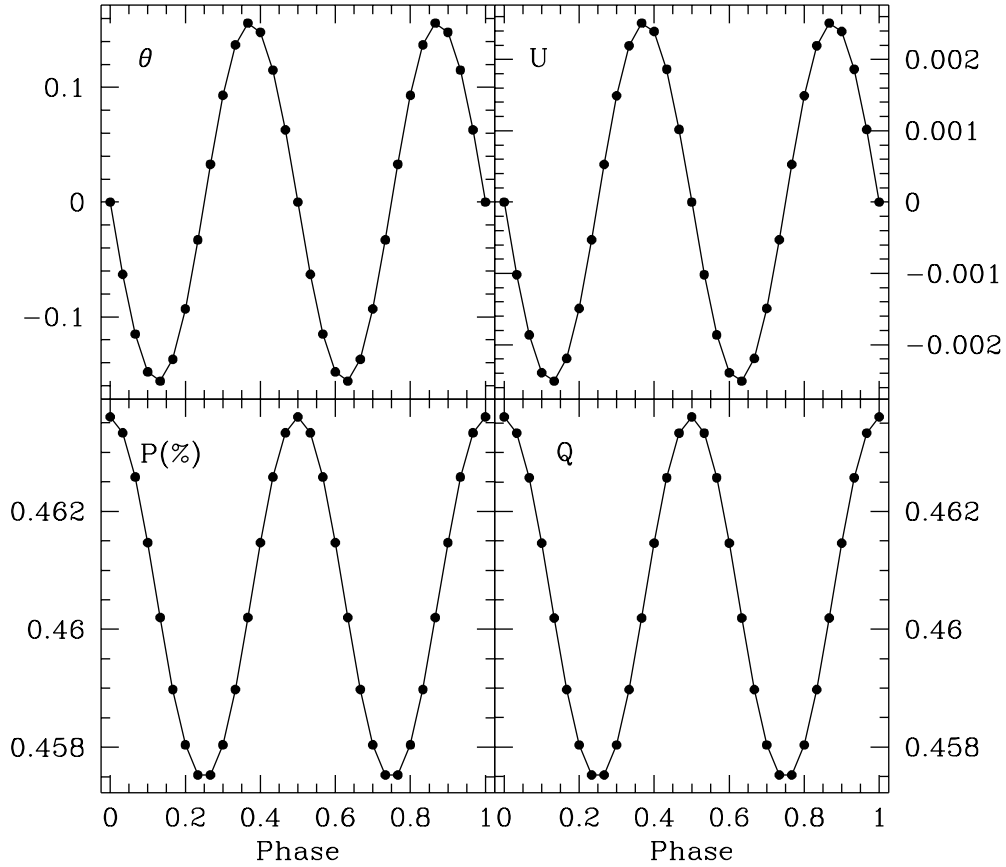


Fig. 3.— Typical simulation for a binary star in a circumbinary envelope: polarization P , position angle θ , Stokes parameters Q and U , as a function of the orbital phase ϕ . We used astronomical silicate grains of $0.1\mu\text{m}$, an optical depth of 0.1, and an inclination of 60° . The polarimetric variations are purely double-periodic.

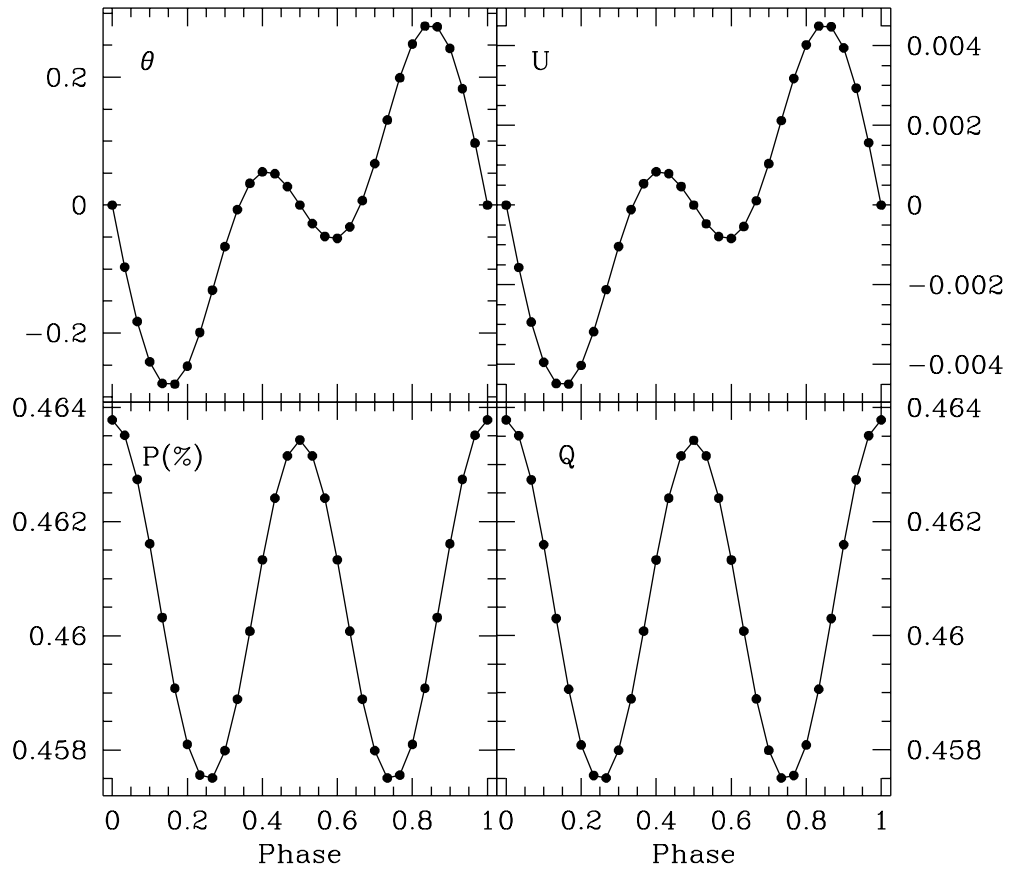


Fig. 4.— Same simulation as the previous figure, taking only the primary star; the secondary is supposed to be much fainter than the primary. In addition to the usual double-periodic variations, single-periodic ones are clearly seen.

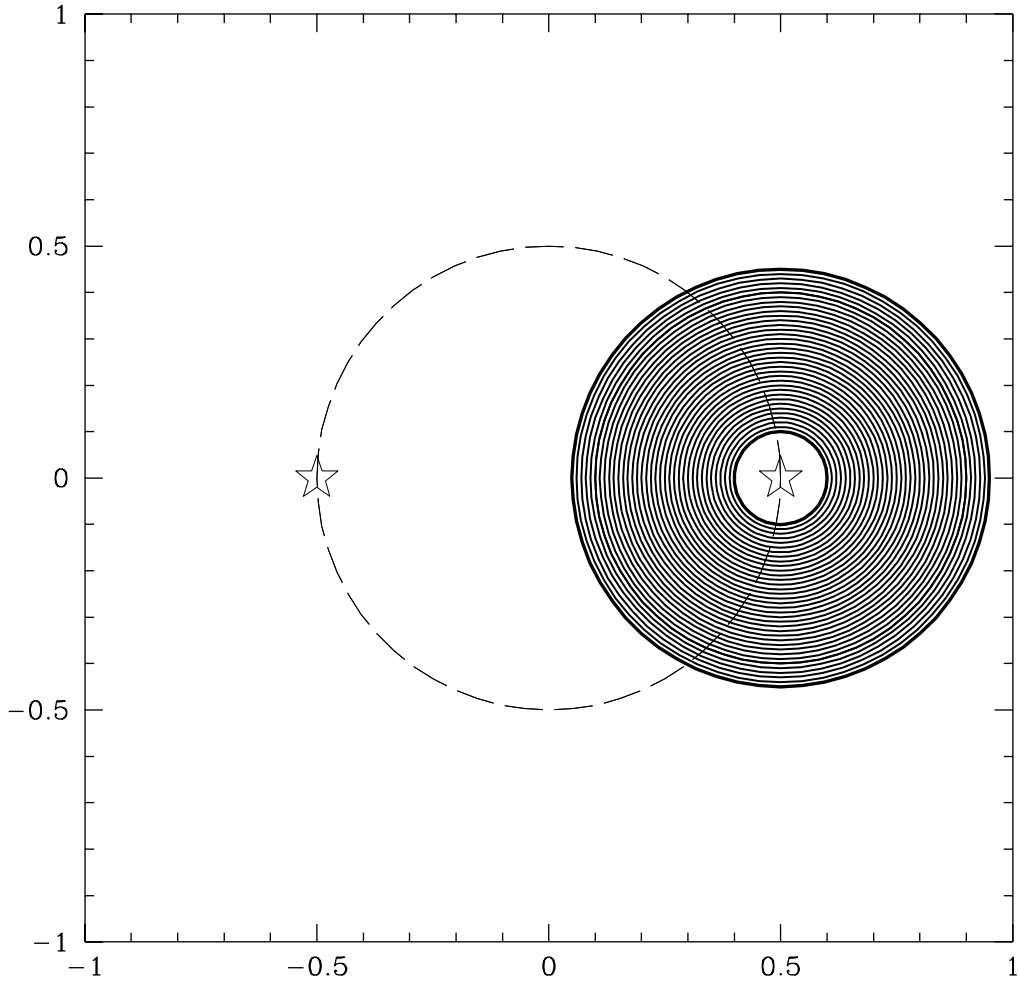


Fig. 5.— Pole-on view of a binary system with only one circumstellar envelope.

Grain Composition	$\Re(m)$	$\Im(m)$ ¹	m
BE (amorphous carbon) ²	2.240	0.781	2.37
Graphite ³	2.524	1.532	2.95
Dirty ice ⁴	1.33	0.09	1.34
Astronomical silicate ⁵	1.715	0.030	1.72

Table 1: Characteristics of dust grains used in the numerical simulations.

¹The imaginary part of the complex refractive index m represents the absorption of radiation by the grains.

References. — (2) Rouleau & Martin 1991; (3) Wickramasinghe & Guillaume 1965; (4) Wickramasinghe 1967; Greenberg 1968; (5) Draine 1985

i_{true}		Electrons	Astron. Silicates	Graphite	Amorphous Carbon	Dirty Ice
90°	P_{ave} (%)	0.794	0.619	0.299	0.270	0.189
	ΔP (%)	0.0063	0.0048	0.0023	0.0021	0.0015
	$P_{\text{ave}}/\Delta P$	0.0079	0.0075	0.0077	0.0078	0.0079
60°	P_{ave} (%)	0.593	0.461	0.222	0.201	0.140
	ΔP (%)	0.0079	0.0061	0.0029	0.0027	0.0018
	$P_{\text{ave}}/\Delta P$	0.0133	0.0132	0.0131	0.0134	0.0129
45°	P_{ave} (%)	0.395	0.306	0.147	0.133	0.093
	ΔP (%)	0.0095	0.0073	0.0035	0.0032	0.0022
	$P_{\text{ave}}/\Delta P$	0.0241	0.0239	0.0238	0.0241	0.0237

Table 2: Average polarization, P_{ave} , and amplitude of the polarimetric variations, ΔP , produced by electrons and different gain compositions, for different orbital inclinations.